RSC Advances

PAPER

View Article Online
View Journal | View Issue

Cite this: *RSC Adv.*, 2026, **16**, 1157

Facile synthesis of Co-based catalysts with high dispersion *via* an eco-friendly strategy

Feng Gu,[a] Guoqing Xiao,[a] Qiuyao Jiao,[a] Yan Liu,*[b] Pengyong Wei[a] and Lei Li *[a]

Received 26th November 2025
Accepted 11th December 2025

DOI: 10.1039/d5ra09134a

rsc.li/rsc-advances

The supported metal catalyst featuring highly dispersed active species poses a challenge for industrial catalysts, even at high loadings. Herein, highly dispersed supported cobalt catalysts were prepared using an impregnation and vacuum-heating strategy. During the vacuum-heating process, coordinated H_2O was removed, restricting the formation of metal-bound OH species and their aggregation, yielding small metal oxide species. The synthesized catalyst shows high cobalt time yield and improved C_{5+} selectivity compared to the catalyst prepared by the traditional impregnation-calcination method. It revealed that more accessible active sites and strong metal–support interaction contributed to superior FTS performance. This study provides a simple, efficient way to prepare supported metal catalysts with high dispersion at an industrial scale.

Introduction

Supported metal catalysts play an important role in many catalytic applications, including the synthesis of fuels and chemicals, energy conversion and storage, and nano-electronics.[1,2] As is well-known, most chemical and electronic processes always occur at the catalyst surface, the intrinsic properties of nanoparticles are closely correlated with particle size, spatial distribution, and crystal shape.[3,4] Thus, it is urgent to develop highly dispersed supported metal catalysts, because small particles can provide abundant active sites for the adsorption/activation of reaction molecules.

In the past decade, various classic strategies have been employed in the synthesis of highly dispersed metal catalysts, such as sol–gel method,[5,6] colloidal synthesis,[7,8] deposition precipitation,[9,10] electrostatic adsorption,[11] encapsulated structures,[12–15] or plasma treatment.[16,17] Despite these strategies being effective, they suffer from inherent disadvantages, including complex synthetic steps, low synthetic yield, excessive chemical use, and difficulty in scaling up. To date, the impregnation method remains the preferred synthetic route in the chemical industry due to its ease of scale-up.[18] However, metal (oxide) aggregation is inevitable *via* an impregnation method even with a low loading (<5 wt%). To address this issue, the Krijn P. de Jong group developed highly dispersed supported metal (oxide) catalysts by carefully controlling the drying process[19] or the heating atmosphere.[20] Drying at 100 °C (the optimum temperature) in N_2 flow resulted in the maximum spacing of the Co_3O_4 nanoparticles, leading to high dispersion rather than aggregation. A calcination atmosphere containing 1% NO/He could prevent the rapid decomposition of cobalt precursors, yielding Co_3O_4 particles with a diameter of 4–5 nm at relatively high loadings. Besides, the surfactant and metal precursor were introduced into the support *via* an impregnation method, in which the surfactant was converted into a carbon source that coated the metal nanoparticles, preventing their sintering during calcination.[21,22] Similarly, a metal–organic ligand rather than a surfactant was used to construct highly dispersed supported metal catalysts.[23–27] On the one hand, the metal precursors and organic ligands are sequentially loaded onto the support, and the interaction effectively inhibits precursor decomposition and the growth of metal oxide nanoparticles.[26,27] On the other side, organometallic complexes or coordination compounds react with well-defined surfaces (*e.g.*, oxides, metal nanoparticles, carbon materials) to achieve the target functionalities on the surface.[23] By combining grafting of precursors on surfaces *via* surface organometallic chemistry with a thermolytic, nonoxidative procedure that removes all organic ligands, isolated atoms may be produced on the surface. However, the use of both ligands and surfactants further increases the complexity and cost of the experiment. Accordingly, developing a general and simple method to prepare supported metal catalysts with high dispersion is highly desirable.

Fischer–Tropsch Synthesis (FTS) is an effective catalytic process for high-value-added chemicals and clean liquid fuels. It is well accepted that cobalt-based catalysts show significant advantages of high activity and selectivity for the production of long-chain hydrocarbons.[28] The FTS catalytic performance strongly depends on cobalt dispersion, reducibility, and stability. Therefore, the balance between particle size and metal

[a]*School of Chemistry and Chemical Engineering, Yancheng Institute of Technology, Yancheng, 224051, PR China. E-mail: lee_ycit@hotmail.com*

[b]*State Key Laboratory of Coal Conversion, Institute of Coal Chemistry, Chinese Academy of Sciences, Taiyuan 030001, Shanxi, PR China. E-mail: liuyan@sxicc.ac.cn*

loading, which correlates with metal reducibility and availability, is very important for maximizing activity.

In this study, we propose a simple, highly effective strategy for preparing well-dispersed supported Co nanocatalysts *via* impregnation followed by vacuum calcination. As illustrated in Fig. 1a, the supported metal catalysts were first prepared by impregnation and dried at low temperature, forming the same precursor/support. Then, it was further calcined by air- and vacuum-heating, respectively. Apparently, the highly dispersed supported metal catalysts were realized using a vacuum-heating strategy rather than an air-heating strategy. This phenomenon should be ascribed to the removal of coordinated H_2O in a vacuum-heating environment, which restricts the formation of metal-bound OH species and their aggregation behavior. The resulting small metal oxide species were not agglomerated into larger particles because of their low mobility and high melting point.[29] It is evident that the immediate removal of water is very important during the preparation process, especially during the whole heating process. In fact, simple vacuum drying could not completely remove coordinated H_2O at low temperatures (*e.g.*, 120 °C), whereas complete removal was achieved at high temperatures (*e.g.*, 450 °C).[20] Meanwhile, it was also indicated that the O_2-free atmosphere significantly reduced aggregation and sintering. Ingeniously, the vacuum-heating strategy proposed in this study can achieve complete and immediate removal of coordinated H_2O and provide an O_2-free calcination environment, effectively reducing the aggregation/sintering of active components on the support.

Experimental

Catalyst preparation

A predetermined mass of cobalt nitrate hexahydrate ($Co(NO_3)_2 \cdot 6H_2O$) was dissolved in distilled water and then impregnated onto supports (*e.g.*, Al_2O_3, ZrO_2, and SiO_2). The support was measured at 4.0 g each time, dispersed in 50 mL deionized water, and then the cobalt salt was added to achieve a theoretical cobalt loading of 20 wt%. The mixture was stirred at room temperature for 6 h. The wet solid was further dried in a conventional oven at 60 °C overnight to remove moisture. After completely drying, the dried sample was pressed into bulk pellets. The bulk pellets were cracked and sieved into small particles of 40–60 mesh. The yield samples were then divided into two parts. One part was calcined under a vacuum system (Plasma-Enhanced Chemical Vapor Deposition, PECVD), BTF-1200C-R-PECVD-AD2, produced by Anhui Best Equipment Technology Co., Ltd. The vacuum level was controlled at around 1 Pa. The calcining temperature was raised from room temperature to 500 °C at 1 °C min^{-1}, then held at 500 °C for 2 h. The prepared catalysts were marked as Co/support-V (*e.g.*, Co/SiO_2-V, Co/ZrO_2-V, and Co/Al_2O_3-V). The other part was directly calcined in a muffle furnace (KSL-1200X-J, Hefei Kejing Material Technology Co., Ltd) with static air. The calcination was performed from room temperature to 500 °C at 1 °C min^{-1}, held at 500 °C for 2 h, and the final catalysts were referred to as Co/support-A (*e.g.*, Co/SiO_2-A, Co/ZrO_2-A, and Co/Al_2O_3-A).

Characterizations

The cobalt-based catalysts were characterized by XRD, TEM, BET, XPS, H_2-TPR/TPD, CO-TPD, and *in situ* FTIR techniques. The detailed methods were described in the SI.

Catalytic performance

The FTS performance of these catalysts was measured on a stainless-steel fixed-bed reactor. The detailed operations were described in the SM.

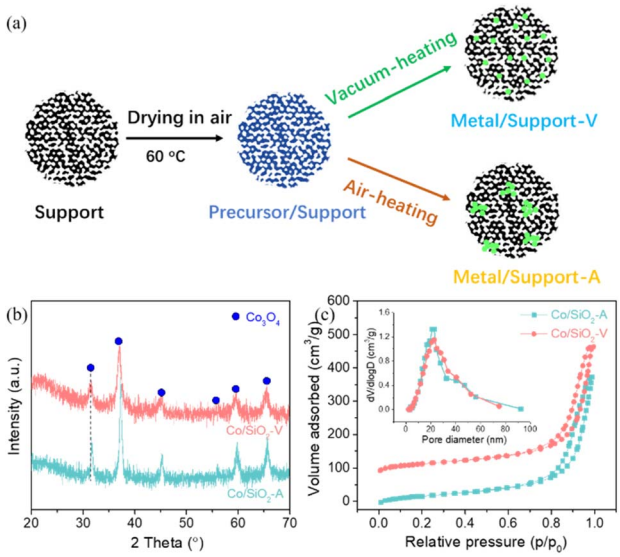

Fig. 1 (a) Schematic of the synthetic strategy for the highly dispersed supported metal catalysts, (b) XRD profiles, and (c) N_2 sorption results of the contrast Co-based samples (Co/SiO_2-A and Co/SiO_2-V).

Results and discussion

XRD patterns of the contrast Co/SiO_2 samples are shown in Fig. 1b. All the distinct diffraction peaks can be well indexed to the cubic phase of Co_3O_4 (JCPDS # : 42-1467). Notably, compared with the Co/SiO_2-A sample, the Co/SiO_2-V sample displays broad and weak diffraction peaks, implying a smaller particle size. Similar results regarding the particle size of Co_3O_4 species were also observed and confirmed over Al_2O_3 and ZrO_2 supports (Fig. S1(a and b)). Furthermore, the mean crystallite sizes of the different samples were calculated using the Scherrer equation based on the diffraction peak at *ca.* 36.8° from Co_3O_4, and the results are listed in Table S1. Clearly, the particle size of Co_3O_4 achieved in the vacuum-heating sample is smaller than that achieved in the air-heating sample. For instance, the average particle sizes of Co_3O_4 in Co/SiO_2-V and Co/SiO_2-A samples are 11.7 and 18.3 nm, respectively. This result aligns with our vision that small particles can be loaded onto the support using a vacuum-heating strategy.

Fig. 1c displays the N_2 adsorption–desorption isotherms and the corresponding pore size distribution curves of the representative catalysts (Co/SiO_2-V and Co/SiO_2-A). Both samples exhibit similar type IV isotherms and hysteresis loops at high

relative pressures, indicating the presence of stacked pores.[30] As listed in Table S1, there exists a slight distinction of surface area, pore volume, and pore size distribution in the serial contrast samples. For instance, the surface area, pore volume, and pore size distribution are *ca.*140 m^2 g^{-1}, 0.6 cm^3 g^{-1}, and 17.5 nm for both Co/SiO_2-V and Co/SiO_2-A samples. As for Co/Al_2O_3-V (or Co/ZrO_2-V) and Co/Al_2O_3-A (or Co/ZrO_2-A) catalysts, they show similar physicochemical properties.

The morphology, structure, and elemental composition of the representative samples (Co/SiO_2-V and Co/SiO_2-A) were studied by TEM and EDS. As shown in Fig. 2, there is an obvious aggregation in the Co/SiO_2-A sample obtained by air-heating, while there is no obvious agglomeration of cobalt oxides in the Co/SiO_2-V sample (Fig. 2a and b). This finding is consistent with XRD analyses. Besides, lattice fringes with interlayer spacings of 0.246 nm and 0.467 nm, corresponding to the (311) and (111) crystal planes of Co_3O_4, were identified (Fig. S2). Seen from the EDS mappings (Fig. 2c–h), the dispersion of cobalt oxides in the Co/SiO_2-A sample is poor, while it exhibits a good dispersion in the Co/SiO_2-V sample. It indicates that the vacuum-heating strategy can effectively inhibit the agglomeration of cobalt species, improving its dispersion and providing more accessible active sites.

The surface chemical states of cobalt species were further investigated using XPS. In Fig. 3a, the Co $2p_{2/3}$ spectra were deconvoluted into three peaks, corresponding to Co^{3+}, Co^{2+}, and the satellite structure of Co^{2+}. Evidently, the intensity of Co^{2+} satellites peaks in the Co/SiO_2-V sample is stronger than that in the Co/SiO_2-A sample. Seen from peak-fitting results (Table S2), the surface molar ratio of Co^{2+}/Co^{3+} in Co/SiO_2-V (0.96) is still larger than that in Co/SiO_2-A (0.81). A previous study indicated that this satellite peak should be ascribed to

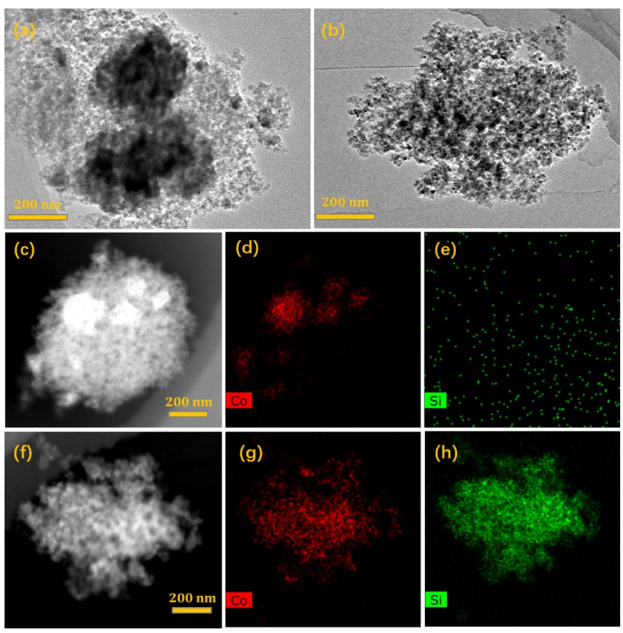

Fig. 2 TEM and EDS images of different catalysts, (a and c–e) Co/SiO_2-A and (b and f–h) Co/SiO_2-V.

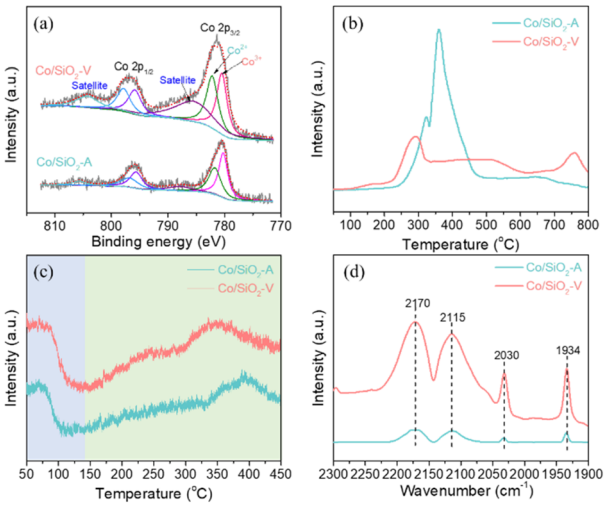

Fig. 3 (a) Co2p XPS spectra, (b) H_2-TPR profiles, (c) H_2-TPD profiles, and (d) FTIR of CO adsorption of different Co/SiO_2 samples.

Co_2SiO_4 rather than surface cobalt species,[31] implying a strong metal–support interaction. This strong interaction could effectively prevent the mobility of active cobalt species, significantly enhancing the long-term stability in the FTS reaction.[26] In Table S2, the surface atomic concentration of Co (2.42 at%) and Co/Si atomic ratio (0.08) in Co/SiO_2-V sample are larger than those in Co/SiO_2-A sample (1.22 at% and 0.04). This result reflects a higher number of exposed Co metal sites in the Co/SiO_2-V sample.[32] More surface-exposed Co metal sites can contribute to superior FTS performance.

The redox property was measured using H_2-TPR. Fig. 3b displays the H_2-TPR profile of the contrast samples (Co/SiO_2-V and Co/SiO_2-A). The reduction peaks are mainly located in the low-temperature range (200–500 °C) and the high-temperature range (above 500 °C). The former corresponds to the continuous reduction from Co^{3+} to Co^{2+} and Co^0, while the latter corresponds to the Co species strongly interacting with silica or $CoSi_2O_4$ species.[30] We also note that the Co/SiO_2-V has a lower reduction temperature but with a small amount of hydrogen consumption compared with the Co/SiO_2-A sample. This phenomenon might be linked to the dual effects of highly dispersed, strongly interacting cobalt species coexisting on the catalyst support. Besides, the H_2-TPR profiles of different Co/Al_2O_3 and Co/ZrO_2 catalysts were also illustrated in Fig. S3. Similarly, the redox behavior also occurs on Al_2O_3-supported cobalt catalyst, especially the high-temperature reduction peak, which should be ascribed to a strong interaction between cobalt and alumina or the formed $CoAl_2O_4$ species.[26] Due to the weak metal–support interaction, only low-temperature range reduction peaks were observed on ZrO_2-supported cobalt catalysts. In general, this vacuum-heating strategy effectively boosts the dispersion of cobalt species and their reduction.

Fig. 3c shows the H_2-TPD profiles in the representative Co/SiO_2-V and Co/SiO_2-A samples, and the hydrogen desorption amounts are placed in Table S3. Clearly, the hydrogen desorption amount of Co/SiO_2-V (38.9 μmol g^{-1}) is more than that of

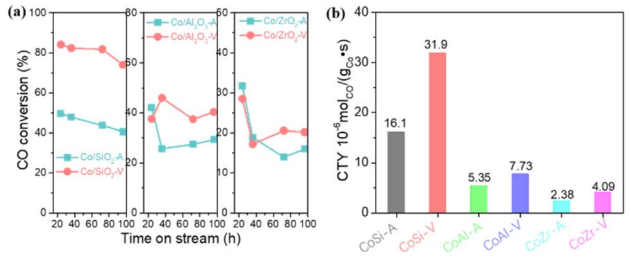

Fig. 4 Catalytic performance of different catalysts. (a) Time-on-stream evaluation of CO conversion. (b) Co-time yields (CTY) at 72 h on stream. Reaction conditions: $T = 200$ °C, $P = 2$ MPa, SV = 1000 h^{-1}, $CO/H_2 = 1/2$.

Co/SiO_2-A (16.9 μmol g^{-1}), implying a significant increase in the number of accessible metallic cobalt sites on the surface. The cobalt atomic dispersions are 0.50% and 1.15% for the Co/SiO_2-A and Co/SiO_2-V samples, respectively. This result correlates well with the above characterizations. Besides, a CO adsorption experiment was performed at room temperature, as detected by *in situ* FTIR (Fig. 3d). The bands at 2173 and 2116 cm^{-1} correspond to gas-phase CO adsorption. The bands at 2070 and 2025 cm^{-1} are attributed to the linear adsorption of CO, while the peak at 1934 cm^{-1} is caused by the bridge adsorption of CO.[33] Notably, the absorption peak intensity of CO in the Co/SiO_2-V sample is stronger than that in the Co/SiO_2-V sample. It indicated that the Co/SiO_2-V sample contains more small cobalt particles, and CO adsorption on small Co particles is significantly stronger than on large Co particles.[34] This is because smaller Co particles contain more low-coordination Co atoms, which interact strongly with CO and have a smaller desorption equilibrium constant.

Fig. 4 shows the FTS activity of different catalysts; the detailed results are listed in Tables 1 and S3. As shown in Fig. 4a, the cobalt-based catalysts prepared by the vacuum-heating strategy are obviously superior to those prepared by air-heating. Due to the different nature of the supports, significant differences in FTS activity are observed, and CO conversion activity follows the order: Co/SiO_2 > Co/Al_2O_3 > Co/ZrO_2. Especially for the Co/SiO_2 catalyst, the stabilized CO conversion is *ca.* 82.0% in Co/SiO_2-V catalyst at a reaction time of 72 h, and the activity is nearly double that of Co/SiO_2-A (*ca.* 43.0%). Accordingly, the mass-specific cobalt time yield (CTY) (3.19×10^{-5} mol_{CO} g_{Co}^{-1} s^{-1}) and TOFs (4.43×10^{-3} s^{-1}) in Co/SiO_2-V catalyst are significantly higher than those of Co/SiO_2-A catalyst (1.61×10^{-5} mol_{CO} g_{Co}^{-1} s^{-1}, 3.33×10^{-3} s^{-1}). As shown in Fig. 4b, the catalysts prepared by vacuum-heating have higher CTY values than the ones prepared by air-heating. Based on the above characterizations, it can be concluded that the super FTS activity strongly depends on the increased number of cobalt active sites, originating from the vacuum-heating strategy. In addition, the strong metal–support interaction, along with the formation of an inactive metal–support spine species (*i.e.*, CoSi and CoAl), would change the geometric structure of the active site.[35] The more efficient utilization of the cobalt–support interface could result in a sharp increase in CTY value. Similarly, for other supports (Al_2O_3 and ZrO_2), catalysts prepared by the vacuum-heating strategy consistently improve or sustain catalytic activity compared to those prepared by the air-heating method, demonstrating the effectiveness and universality of this strategy for preparing highly supported metal catalysts.

The CO-TPD profiles over the contrast catalysts were measured (Fig. S4). The desorption peaks were mainly centered at 50–150 °C and 200–600 °C, corresponding to the desorption of CO molecules (CO_{ads}) and the CO (CO*) through the recombination of dissociated C* and O*, respectively.[33,36] Notably, the CO desorption peak in Co/SiO_2-V shifts to a lower temperature compared with Co/SiO_2-A. It indicates that there exists fast dissociation and recombination behavior of C* and O* in Co/SiO_2-V catalyst, which might improve FTS activity through carbide mechanism.[37] Besides, the selectivity of products over different catalysts was also listed in Tables 1 and S3. We found that the Co/SiO_2-V catalyst favors the yield of long-chain hydrocarbons (C_{5+} selectivity = 92.34%) while suppressing methane formation (CH_4 selectivity = 3.63%). By comparison, the Co/SiO_2-A catalyst exhibits lower C_{5+} selectivity (83.91%) and higher methane selectivity (7.31%). Similar results were also observed for Al_2O_3- and ZrO_2-supported catalysts. It was reported that the optimum cobalt particle size (6–10 nm) could affect the selectivity of C_{5+} with a critical value.[35] Thus, the superior selectivity of the vacuum-heating prepared catalysts should be assigned to the higher density of metallic cobalt sites and the modified surface structures, which potentially facilitate the chain growth for long-chain alkanes. In addition, some representative Co-based catalysts for the FTS were listed in Table S4. Although the previously reported catalysts were evaluated under different reaction conditions, our as-prepared catalysts exhibited high CO conversion and high selectivity for long-chain paraffins.

Table 1 Catalytic performance of the typical Co/SiO_2 catalysts

Catalyst	Conv. (CO)[a]/%	S(CH_4)/%	S(C_2–C_4)/%	S(C_{5+})/%	H_2 desorbed (μmol g^{-1})	Dispersion[b] (%)	CTY (10^{-5} $mol_{CO}/(g_{Co}$ $s^{-1})$)	TOFs[c] (10^{-3} s^{-1})
Co/SiO_2-A	43.66	7.31	8.77	83.91	16.9	0.50	1.61	3.33
Co/SiO_2-V	81.86	3.63	4.03	92.34	38.9	1.15	3.19	4.43

[a] The data of the seventh day (stable for 72 h) were selected. Reaction condition: $T = 200$ °C, $P = 2$ MPa, GHSV = 1000 h^{-1}, $H_2/CO = 2$. [b] The H_2 desorption amounts and dispersion were calculated from H_2-TPD results. [c] The TOF values were calculated by the conversion rate and metal Co dispersion.

Conclusions

In summary, we proposed a general, simple synthetic strategy for highly dispersed supported metal catalysts, even at high loadings. The vacuum-heating strategy was employed to rapidly remove coordinated H_2O from the metal salt precursor, thereby restricting the formation of metal-bound OH species and their aggregation, yielding small metal oxide species. Compared with the traditional air-heating method, the resultant cobalt catalysts supported on different supports (*i.e.*, SiO_2, Al_2O_3, ZrO_2) show excellent FTS activity and high selectivity to C_{5+} product. The increased metal dispersion and metal–support interaction contribute to this superior performance. This study provides a simple, efficient way to prepare supported metal catalysts with high dispersion at an industrial scale.

Author contributions

Feng Gu: methodology, investigation, supervision, resources. Guoqing Xiao: investigation, data curation, discussion. Qiuyao Jiao: methodology, data curation, writing – original draft. Yan Liu: supervision, resources. Pengyong Wei: formal analysis, data curation. Lei Li: supervision writing – review & editing.

Conflicts of interest

The authors declare that they have no known competing financial interests or personal relationships that could have influenced the work reported in this paper.

Data availability

The data supporting this article are included in the supplementary information (SI). Supplementary information: experimental section; XRD patterns of different Co/Al_2O_3 and Co/ZrO_2 catalysts; HRTEM images of Co/SiO_2-A and Co/SiO_2-V catalysts; H2-TPR profiles of different Co/Al_2O_3 and Co/ZrO_2 catalysts; CO-TPD profile of different Co/SiO_2 catalysts; Table S1: Physchemical properties of different catalysts; Table S2: XPS results of different Co/SiO_2 catalysts; Table S3: catalytic performance of different Co/Al_2O_3 and Co/ZrO_2 catalysts; Table S4: the FTS performance of the representative Co-based catalysts. See DOI: https://doi.org/10.1039/d5ra09134a.

Acknowledgements

This work was supported by the Natural Science Foundation of Shanxi Province (No. 202303021221258). And the Talent Introduction Project of Yancheng Institute of Technology. And the Postgraduate Research & Practice Innovation Program of Yancheng Institute of Technology (KYCX25 XZ008).

Notes and references

1 H. M. Torres Galvis, J. H. Bitter, C. B. Khare, M. Ruitenbeek, A. I. Dugulan and K. P. De Jong, *Science*, 2012, **335**, 835–838.
2 C. Galeano, J. C. Meier, V. Peinecke, H. Bongard, I. Katsounaros, A. A. Topalov, A. Lu, K. J. J. Mayrhofer and F. Schüth, *J. Am. Chem. Soc.*, 2012, **134**, 20457–20465.
3 A. T. Bell, G. C. Bond, D. T. Thompson, M. Valden, X. Lai, D. W. Goodman, T. Blasko, J. M. L. Nieto, K. Chen, A. T. Bell, E. Iglesia, T. Koyama, T. Komaya, P. L. Gai, M. Weyland, G. Durscher, N. D. Browning, S. J. Pennycook, F. Besenbacker, P. C. Thune, J. Loss, D. Wonter, P. J. Leustra, J. W. Niemantsverdriet, J. Corker, V. Vidal, A. Theolier, J. Thivolle-Cazat, J.-M. Basset, C. Nozkaki, C. G. Lugmair, A. T. Bell, T. D. Tilley, D. Kolb, K. P. De Jong and J. W. Geus, *Science*, 2003, **299**, 1688–1691.
4 T. M. Eggenhuisen, J. P. den Breejen, D. Verdoes, P. E. de Jongh and K. P. de Jong, *J. Am. Chem. Soc.*, 2010, **132**, 18318–18325.
5 J. D. Mackenzie and E. P. Bescher, *Acc. Chem. Res.*, 2007, **40**, 810–818.
6 J. Liu, S. Zou, S. Li, X. Liao, Y. Hong, L. Xiao and J. Fan, *J. Mater. Chem. A*, 2013, **1**, 4038–4047.
7 H. Winnischofer, T. C. R. Rocha, W. C. Nunes, L. M. Socolovsky, M. Knobel and D. Zanchet, *ACS Nano*, 2008, **2**, 1313–1319.
8 S. G. Kwon and T. Hyeon, *Acc. Chem. Res.*, 2008, **41**, 1696–1709.
9 J. Cho, L. Xu, C. Jo and R. Ryoo, *Chem. Commun.*, 2017, **53**, 3810–3813.
10 Y. Soni, I. Kavya, T. G. Ajithkumar and C. P. Vinod, *Chem. Commun.*, 2018, **54**, 12412–12415.
11 L. Jiao and J. R. Regalbuto, *J. Catal.*, 2008, **260**, 329–341.
12 Z. Bian, Z. Li, J. Ashok and S. Kawi, *Chem. Commun.*, 2015, **51**, 16324–16326.
13 G. Wang, S. Xu, L. Wang, Z. Liu, X. Dong, L. Wang, A. Zheng, X. Meng and F.-S. Xiao, *Chem. Commun.*, 2018, **54**, 3274–3277.
14 L. Li, S. He, Y. Song, J. Zhao, W. Ji and C. T. Au, *J. Catal.*, 2012, **288**, 54–64.
15 Z. Li, L. Mo, Y. Kathiraser and S. Kawi, *ACS Catal.*, 2014, **4**, 1526–1536.
16 Z. Wang, Y. Zhang, E. C. Neyts, X. Cao, X. Zhang, B. W. L. Jang and C. J. Liu, *ACS Catal.*, 2018, **8**, 2093–2110.
17 J. Hong, J. Du, B. Wang, Y. Zhang, C. Liu, H. Xiong, F. Sun, S. Chen and J. Li, *ACS Catal.*, 2018, **8**, 1591–1600.
18 P. Munnik, P. E. De Jongh and K. P. De Jong, *Chem. Rev.*, 2015, **115**, 6687–6718.
19 P. Munnik, P. E. De Jongh and K. P. De Jong, *J. Am. Chem. Soc.*, 2014, **136**, 7333–7340.
20 J. R. A. Sietsma, J. D. Meeldijk, J. P. Den Breejen, M. Versluijs-Helder, A. J. Van Dillen, P. E. De Jongh and K. P. De Jong, *Angew. Chem., Int. Ed.*, 2007, **46**, 4547–4549.
21 W. Zhan, Q. He, X. Liu, Y. Guo, Y. Wang, L. Wang, Y. Guo, A. Y. Borisevich, J. Zhang, G. Lu and S. Dai, *J. Am. Chem. Soc.*, 2016, **138**, 16130–16139.
22 S. Das, A. Jangam, Y. Du, K. Hidajat and S. Kawi, *Chem. Commun.*, 2019, **55**, 6074–6077.
23 M. K. Samantaray, V. D'Elia, E. Pump, L. Falivene, M. Harb, S. Ould Chikh, L. Cavallo and J.-M. Basset, *Chem. Rev.*, 2020, **120**, 734–813.

24 O. Sodpiban, T. Kessaratikoon, J. Smith, G. Ren, S. Del Gobbo, S. Das, M. Chi, V. D'Elia and B. C. Gates, *ACS Appl. Mater. Interfaces*, 2023, **15**, 55885–55894.
25 M. P. Conley, M. F. Delley, F. Núñez-Zarur, A. Comas-Vives and C. Copéret, *Inorg. Chem.*, 2015, **54**, 5065–5078.
26 Y. Liu, L. Li, J. Zhang and B. Hou, *Fuel*, 2024, **375**, 132569.
27 L. Li, Q. Yang, B. Wang, D. Wang, Y. Peng, J. Li and J. Crittenden, *J. Cleaner Prod.*, 2021, **278**, 123920.
28 Z. Gholami, Z. Tišler and V. Rubáš, *Catal. Rev. – Sci. Eng.*, 2021, **63**, 512–595.
29 P. Yan, S. Xi, H. Peng, D. R. G. Mitchell, L. Harvey, M. Drewery, E. M. Kennedy, Z. Zhu, G. Sankar and M. Stockenhuber, *J. Am. Chem. Soc.*, 2023, **145**, 9718.
30 L. Li, Y. Liu, J. Zhang, M. Xia and W. Ji, *Fuel*, 2022, **329**, 125481.
31 X. Li, Y. Chen, M. U. Nisa and Z. Li, *Appl. Catal., B*, 2020, **267**, 118377.
32 M. Zhong, J. Wang, C. Chen, Z. Ma, L. Jia, B. Hou and D. Li, *Catal. Sci. Technol.*, 2019, **9**, 6037–6046.
33 Q. Jiao, Y. Liu, R. Yu and L. Li, *New J. Chem.*, 2025, **49**, 14373–14380.
34 C. Qiu, B. Wu, S. Meng and Y. Li, *Acta Chim. Sin.*, 2015, **73**, 690–698.
35 T. Lin, Y. An, F. Yu, K. Gong, H. Yu, C. Wang, Y. Sun and L. Zhong, *ACS Catal.*, 2022, **12**, 12092–12112.
36 R. P. Galhenage, H. Yan, A. S. Ahsen, O. Ozturk and D. A. Chen, *J. Phys. Chem. C*, 2014, **118**, 17773–17786.
37 K. T. Rommens and M. Saeys, *Chem. Rev.*, 2023, **123**, 5798–5858.